RNA Folding and RNA–Protein Binding Analyzed by Fluorescence Anisotropy and Resonance Energy Transfer

CHAPTER · DECEMBER 2007

DOI: 10.1007/0-387-23690-2_10

1 AUTHOR:

Gerald M Wilson
University of Maryland, Baltimore
87 PUBLICATIONS **3,161** CITATIONS

Full citation: Wilson, G.M. (2005) "RNA folding and RNA-protein binding analyzed by fluorescence anisotropy and resonance energy transfer", in Reviews in Fluorescence, Vol. 2, Geddes, C.D. and Lakowicz, J.R., eds., Springer Science+Business Media, Inc., New York, NY, pp. 223-243.

RNA FOLDING AND RNA-PROTEIN BINDING ANALYZED BY FLUORESCENCE ANISOTROPY AND RESONANCE ENERGY TRANSFER

Gerald M. Wilson*

10.1. INTRODUCTION

Ribonucleic acids (RNA) perform a host of functions in all living things. The vast majority of these roles are associated with diverse aspects of gene expression, including but not limited to delivery of genetic information between the genome (usually DNA) and protein synthetic machinery, coordination of processing events on nascent RNA molecules, and delivery of amino acids to translating ribosomes, which themselves are largely composed of RNA. More recent concepts in RNA metabolism include *cis*-regulation of gene expression by riboswitches[1] and *trans*-regulation through small, noncoding RNAs[2]. Over the past two decades, a large body of work has described catalytic functions for many RNA molecules, from small structured RNAs capable of self-cleavage to the peptidyltransfer functions of ribosomes[3, 4]. Finally, the heterogeneous nature of RNA structure and its amenability to reiterative selection procedures has prompted significant biotechnological interest in RNA aptamers. These are generally short RNA sequences that exhibit high affinity and selectivity for specific molecular targets, and show considerable promise as tools for diagnostic sensing and modulation of biomolecular function[5, 6].

A unique feature of RNA that lends itself to functional complexity in biological systems is that RNA molecules, while encoded by double-stranded DNA templates, are themselves synthesized without a complimentary strand. The plethora of hydrogen bond potential presented by single-stranded RNA molecules thus provides myriad possibilities for conformational variation through intra- and inter-molecular hybridization[7]. Furthermore, many biological functions of RNA are mediated through interactions with sequence-specific RNA-binding proteins. In this review, I describe steady-state fluorescence-based strategies for quantitative analyses of RNA folding and RNA-protein binding events, along with the merits and limitations of these techniques relative to alternative

*Gerald M. Wilson, Department of Biochemistry and Molecular Biology and Center for Fluorescence Spectroscopy, University of Maryland School of Medicine, 108 N. Greene St., Baltimore, MD 21201; Tel: (410)706-8904; Fax: (410)706-8297; e-mail: gwils001@umaryland.edu.

methods. Finally, I summarize some recent progress in the study of mechanisms directing cytoplasmic mRNA decay that has been facilitated by fluorescence approaches, and briefly consider some new frontiers that will permit analyses of RNA structure and function at previously unattainable levels of complexity and subtlety.

10.2. METHODOLOGY

10.2.1. Site-specific Labeling of RNA Substrates with Fluorophores

In general, assessment of RNA folding or protein-binding events by fluorescence spectroscopy requires the conjugation of one or more fluorescent dyes to the substrate RNA molecule. For many cases, this task has been simplified by recent improvements in the quality and cost-effectiveness of solid-phase polyribonucleotide synthesis, and the concomitant proliferation of commercial sources offering such services. We have obtained custom RNA substrates up to 80 nucleotides in length from Dharmacon Research (Lafayette, CO), and selected shorter oligoribonucleotides from Integrated DNA Technologies (Coralville, IA) and others. Both of the abovementioned suppliers offer a number of options for 5'-fluorophore conjugation to synthetic RNA substrates, including fluorescein (Fl), cyanine 3 (Cy3), cyanine 5 (Cy5), and rhodamine (TAMRA). Dharmacon

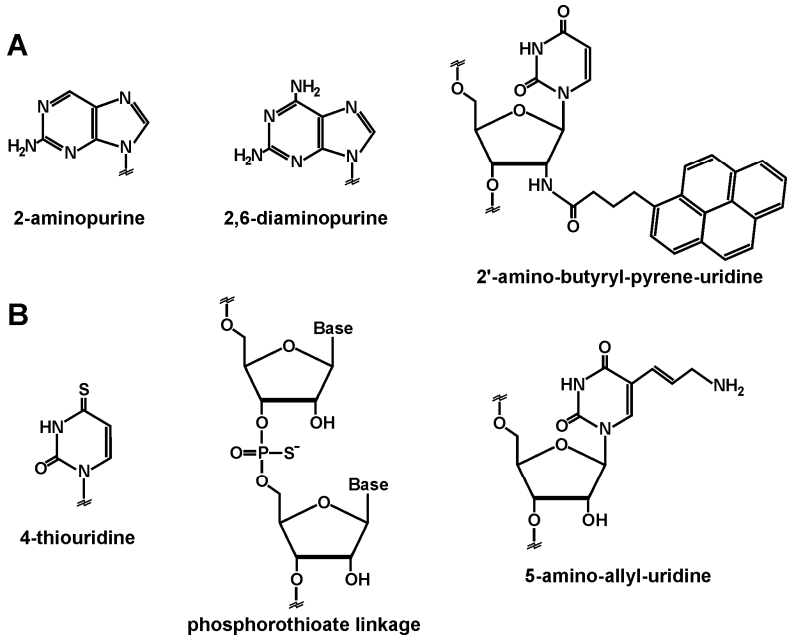

Figure 10.1. (A) Selected fluorescent bases and nucleotides available for incorporation by solid-phase RNA synthesis, and (B) bases and nucleotides permitting conjugation of extrinsic fluorophores at internal sites within synthetic oligoribonucleotides.

further offers each of these fluorophores as 3'-conjugates. At present, incorporation of fluorescent dyes at internal sites on RNA substrates is largely limited to the ultraviolet-excited probes 2-aminopurine and 2,6-diaminopurine (Figure 10.1A). Recently, Dharmacon also began offering site-specific incorporation of a uridine analogue containing a 2'-amide-linked pyrene.

Incorporation of different fluorophores at either terminus, internally, or in the context of larger (> 80 nucleotides) RNA substrates generally require more elaborate synthetic strategies. For oligonucleotides up to 80 nucleotides, incorporation of 5'- or 3'-terminal amino or thiol groups during solid-phase synthesis readily permits subsequent linkage to fluorophores in the form of *N*-hydroxysuccinymidyl (NHS) esters (for amino groups) or maleimide/iodoacetimide conjugates (for thiol groups). A host of suitable fluorescent dyes with excitation/emission wavelengths spanning both the ultraviolet and visible spectra are available from Molecular Probes (Eugene, OR). Similarly, inclusion of functional groups at specific internal locations within custom-synthesized RNA substrates provides additional opportunities for conjugation of extrinsic fluorophores. For example, 4-thiouridine has been used for base-specific linkage of thiol-reactive probes[8]. Substituting a phosphorothioate group for the generic phosphodiester linkage at a specific point in the RNA polymer may permit similar fluorescent dyes to be targeted to the RNA backbone. Dharmacon also offers to site-specifically incorporate 5-amino-allyl-uridine for conjugation of NHS ester-linked fluorophores (Figure 10.1B).

We prepare fluorescent-labeled RNA substrates larger than 80 nucleotides by one of two principal strategies. The first applies when a single fluorescent dye is required at either the 5'- or 3'-terminus. In this case, the applicable RNA is first synthesized by *in vitro* transcription from a double-stranded DNA template. 5'-labeling is performed by removal of the 5'-triphosphate with alkaline phosphatase, then incorporation of a thiophosphate group on the 5'-OH using adenosine 5'-[γ-thio]triphosphate (ATPγS) and T4 polynucleotide kinase[9]. A fluorophore is then linked to the thiophosphate group as a maleimide conjugate. In our hands, this method typically achieves 20-30% labeling efficiency. Attachment of fluorescent dyes to RNA 3'-termini is achieved by oxidation of

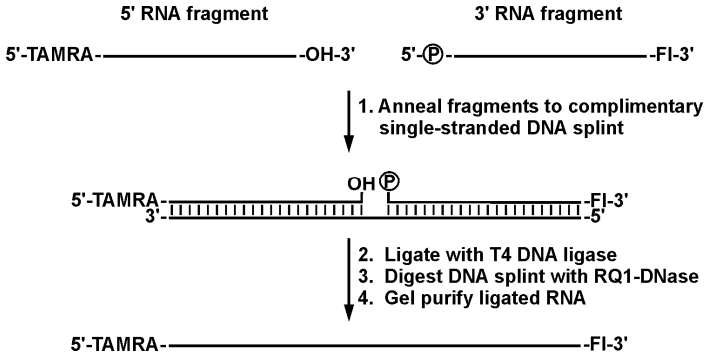

Figure 10.2. Tandem linkage of RNA fragments using single-stranded DNA splints to generate an extended, double-labeled RNA substrate.

the 2',3'-vicinal diol with periodate, then reaction of the resulting dialdehyde with hydrazine-coupled fluorophores. This method achieves labeling efficiencies approaching 100%, and has been reviewed at length elsewhere[10]. The second strategy applies to extended substrates requiring internal or multiple fluorescent dyes linked to a common RNA molecule. In these cases, RNA substrates are generally synthesized in two or three segments, involving solid-phase synthesis and/or *in vitro* transcription. Following incorporation of appropriate fluorophores or functional groups into each segment using the strategies described above, the fragments are assembled by DNA splint-directed ligation and purified (Figure 10.2). A variant of this technique that permits selective incorporation of 4-thiouridine at junction sites has also been described[11].

10.2.2. Assessment of RNA-protein Interactions by Fluorescence Anisotropy

10.2.2.1. Comparison with Alternative Strategies

Many biological functions of RNA, particularly those pertaining to the regulation or utilization of genetic information, involve interactions with cellular proteins[12-15]. Discrimination of binding mechanisms and elucidation of cognate thermodynamic and kinetic parameters require quantitative assay systems to monitor RNA:protein binding events. While we and others have employed gel mobility shift assays (GMSAs) for this purpose[16-18], we find that complex dissociation during electrophoresis often leads to underestimation of solution binding affinity. This limitation is particularly significant for highly dynamic binding events[19]. Similarly, nitrocellulose filter-binding strategies to separate protein-bound from -unbound RNA substrates require washing steps to minimize nonspecific RNA retention[20], during which the equilibrium is modified by lowering the effective concentration of each reagent. In our hands, filter-binding assays also show a high degree of retention for some RNA substrates, even in the absence of protein. Finally, both GMSAs and filter-binding assays suffer from the limitation that reaction components are not measured in free, aqueous solution; in GMSAs, the products are resolved by prolonged passage through a semi-solid (usually polyacrylamide) matrix, while filter-binding assays retain products in the solid phase. An additional method for monitoring RNA-protein equilibria that has recently gained prominence is surface plasmon resonance (SPR), also referred to as BIACORE analysis[21]. However, use of this assay is complicated by three principal limitations. First, one reagent must be affixed to the assay tube, essentially placing the ligand in the solid phase, rather than fully solvated in solution. Heterogeneity in substrate linkage with this surface can generate very complex populations of binding activities, which have been described in some cases by fractal analyses[22]. Second, SPR measurements are kinetic, so equilibrium constants must be derived from the quotient of the on- and off-rates. While this quotient yields the equilibrium constant in ideal cases, the matter becomes more complex for multi-phasic reactions, since multiple, interrelated on- and off-rates must be extracted. The accuracy of the on- and off-rates is also likely influenced by the limitations on ligand diffusion imposed by linking the molecule to a solid support; namely, that the tethered molecule would experience retarded rotational and translational motions. Finally, data analysis must also account for discontinuous fluid dynamics through the assay tube, since frictional interactions between the liquid and solid phases may cause fluids to flow more slowly near the walls of a tube

as compared to its center. Since apparent association/dissociation rates will be influenced by the rate of substrate presentation, this factor should also be considered when extracting equilibrium binding data from SPR experiments.

In light of these considerations, we have employed fluorescence anisotropy to evaluate RNA-protein interactions. Using this system, protein binding to a fluorescent RNA substrate may be detected by the change in fluorescence anisotropy resulting from increases in molecular volume and/or decreases in RNA flexibility[19, 23, 24]. For quantitative evaluation of macromolecular binding, this system offers several advantages over other techniques. First, fluorescence measurements may be taken under true equilibrium conditions, since reaction products are not fractionated (unlike GMSAs or filter-binding). Second, since all reaction components are in solution, this detection method is not complicated by heterogeneity in ligand presentation or solvation (unlike SPR). Third, anisotropy may be measured under both steady-state and pre-steady-state conditions, thus permitting independent assessment of thermodynamic and kinetic reaction parameters (unlike all methods listed above). Fourth, binding assays are logistically simplified by abrogating the need for radioactive compounds to track reaction products (unlike GMSAs or filter-binding). Finally, the mathematical relationships describing fluorescence anisotropy across mixed populations of fluorescent molecules have been well described[25, 26], thus permitting more complex mechanisms of macromolecular interaction such as sequential or cooperative binding events to be quantitatively considered and compared.

10.2.2.2. Theoretical and Practical Considerations

Several of the RNA-binding factors under investigation in our laboratory utilize sequential binding events to form oligomeric structures on RNA substrates (Figure 10.3). Accordingly, we have used this generic framework to develop algorithms for elucidation

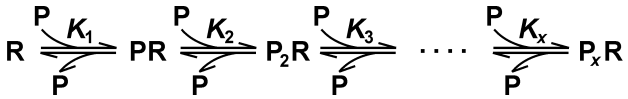

Figure 10.3. Sequential binding model for assembly of an oligomer of *x* protein molecules (P) on a common RNA substrate (R). Thermodynamics of individual binding steps are described by distinct association equilibrium constants (*K*).

of equilibrium binding constants from data generated by fluorescence anisotropy measurements. In practice, a wide variety of RNA-protein binding events may be considered using subsets of this general model. The steady-state concentration of each RNA:protein complex is related to the concentrations of free RNA ([R]), free protein ([P]), and relevant association equilibrium constants by:

$$[PR] = [R][P]K_1$$
$$[P_2R] = [R][P]^2 K_1K_2$$
$$\downarrow$$
$$[P_xR] = [R][P]^x \cdot \prod_{i=1}^{x} K_i$$

Scheme 10.1

Under conditions of constant fluorescence quantum yield, the total measured anisotropy (A_t) of a mixture of fluorescent species labeled with a common fluorophore may be interpreted by Eq. (1)[25, 27, 28].

$$A_t = \sum_i A_i f_i \qquad (1)$$

Here, A_i represents the intrinsic anisotropy of each fluorescent species and f_i its fractional concentration. Applying this function to binding reactions containing fluorophore-coupled RNA substrates and unlabeled proteins, the relevant fractional concentrations of fluorescent reaction components are given by Eq. (2), where $[R]_{tot}$ is the total concentration of RNA substrate in the binding reaction.

$$f_R = \frac{[R]}{[R]_{tot}};\ f_{PR} = \frac{[PR]}{[R]_{tot}};\ \ldots;\ f_{PxR} = \frac{[P_xR]}{[R]_{tot}} \qquad (2)$$

Substitution into Eq. (1) yields:

$$A_t = \frac{1}{[R]_{tot}}\left(A_R[R] + A_{PR}[PR] + \cdots + A_{PxR}[P_xR]\right) \quad (3)$$

Incorporating Scheme 1 and the conservation of mass given in Eq. (4) thus yields the general relationship between A_t and free protein concentration [P] given in Eq. (5).

$$[R]_{tot} = [R] + [PR] + \cdots + [P_xR] \qquad (4)$$

$$A_t = \frac{A_R + A_{PR}[P]K_1 + \cdots + A_{PxR}[P]^x \prod_{i=1}^{x} K_i}{1 + [P]K_1 + \cdots + [P]^x \prod_{i=1}^{x} K_i} \qquad (5)$$

For practical application of this algorithm, $[R]_{tot}$ must be limiting, and in general should be at least 5-fold lower than any K_d (= $1/K$) value. Under these circumstances, the total concentration of protein in the reaction system ($[P]_{tot}$) closely approximates the free protein concentration ([P]), thus permitting solution of reaction parameters by nonlinear regression of A_t versus $[P]_{tot}$ data sets. While many commercially available software

packages adequately resolve such algorithms, we have found the PRISM package (GraphPad, San Diego, CA) particularly useful for these analyses, based on both ease of equation customization and ample assessment of uncertainties in regression solutions.

The simplest type of RNA-protein interaction is the reversible, binary association of a single protein molecule with an RNA substrate described by a single equilibrium constant (ie: $x = 1$). By this model, Eq. (5) thus resolves to:

$$A_t = \frac{A_R + A_{PR}K[P]}{1 + K[P]} \qquad (6)$$

The intrinsic anisotropy of the unbound RNA substrate (A_R) may be measured directly from binding reactions lacking added protein, while the remaining constants (A_{PR}, K) are resolved by nonlinear regression of A_t *versus* [P] ($\approx [P]_{tot}$) data sets. An example of this model is given by the association of the heat shock protein, Hsp70, with an AU-rich RNA substrate (Section 3).

Solutions of A_t *versus* [P] involving two distinct binding steps ($x = 2$) are described by Eq. (7).

$$A_t = \frac{A_R + A_{PR}K_1[P] + A_{P2R}K_1K_2[P]^2}{1 + K_1[P] + K_1K_2[P]^2} \qquad (7)$$

Interaction of the mRNA-destabilizing factor, AUF1, with selected AU-rich RNA substrates is well described by this model (Section 3). While A_R is measured independently of protein as described for Eq. (6), the remaining constants (A_{PR}, A_{P2R}, K_1, and K_2) can generally be well resolved from A_t *versus* [P] provided saturation is approached at high protein concentrations (for approximation of A_{P2R}), and association binding constants differ by a factor of at least 5, with $K_1 > K_2$. When K_2 approaches or is greater than K_1, resolution of a concise solution is hampered by difficulties in establishing the intrinsic anisotropy of the intermediate complex (A_{PR}), largely owing to compensatory influences of A_{PR} and K_2 on regression convergence. However, this limitation can be overcome if an independent measure of either constant is available, as may be obtained by use of selected protein or RNA mutants under some circumstances[19]. Similarly, application of the general model described by Eq. (5) when $x > 2$ is complicated by the large number of reaction parameters requiring resolution. In such cases, values for selected A_{PxR} or K_x constants must generally be obtained in independent experiments using mutant components or reaction conditions which limit x. Subsequently, the remaining reaction parameters may be resolved by global analyses of A_t *versus* [P] data sets.

In some cases, resolution of independent association constants for multi-step binding equilibria may be overly odious or even unnecessary when relative differences in binding activities are under investigation. This is particularly apparent in cooperative protein binding mechanisms, where intrinsic anisotropy values are difficult to assess for intermediate protein:RNA complexes, largely due to their low fractional concentrations. Under these circumstances, we have considered reversible interactions between multiple protein molecules with a fluorescent RNA substrate using the general scheme:

$$x\mathrm{P} + \text{Fl-RNA} \rightleftharpoons \mathrm{P}_x\cdot\text{Fl-RNA}$$

Scheme 10.2

Under conditions where RNA concentration is limiting (ie: $[\mathrm{P}]_{free}$. $[\mathrm{P}]_{total}$), A_t remains dependent on total protein concentration, but may be resolved by a variant of the Hill model[29]:

$$A_t = \frac{A_\mathrm{R} + A_\mathrm{complex} K[\mathrm{P}]^h}{1 + K[\mathrm{P}]^h} \qquad (8)$$

In this model, K represents an aggregate equilibrium constant, h is the Hill co-efficient, and A_R and A_complex are the intrinsic anisotropy values of the free and maximally protein-associated fluorescent RNA substrates, respectively. Adapting a transformation of the Hill model[30] to A_t *versus* [P] data sets returns an additional parameter, $[\mathrm{P}]_{1/2}$, which approximates the concentration of protein yielding half-maximal binding saturation:

$$A_t = A_\mathrm{R} + \left(A_\mathrm{complex} - A_\mathrm{R}\right) \times \left[\frac{\left([\mathrm{P}]/[\mathrm{P}]_{1/2}\right)^h}{1 + \left([\mathrm{P}]/[\mathrm{P}]_{1/2}\right)^h}\right] \qquad (9)$$

Association of Hsp70 with polyuridylate RNA substrates is well described by this model (Section 3).

To this point, all binding algorithms described have assumed that RNA concentrations are limiting, thus permitting the approximation $[\mathrm{P}]_{free}$. $[\mathrm{P}]_{total}$. With readily available instrumentation and high quantum yield fluorophores, this condition generally holds for binding events where $K_\mathrm{d} > 1$ nM. However, in some circumstances, the affinity of selected RNA-binding proteins for cognate substrates may exceed this limit[31]. In such situations, reversible, binary binding events may be resolved in terms of the total concentrations of RNA and protein in the system[26]:

$$A_t = A_\mathrm{R} + (A_\mathrm{PR} - A_\mathrm{R}) \times \left[\frac{1 + K[\mathrm{R}]_{tot} + K[\mathrm{P}]_{tot} - \sqrt{\{(1 + K[\mathrm{R}]_{tot} + K[\mathrm{P}]_{tot})^2 - 4[\mathrm{R}]_{tot}[\mathrm{P}]_{tot}K^2\}}}{2K[\mathrm{R}]_{tot}}\right] \qquad (10)$$

A second condition of the aforementioned binding algorithms is that all reaction products exhibit similar fluorescence quantum yields. This condition ensures that each fluorescent species (ie: R *versus* PR) makes an equivalent molar contribution to total fluorescence emission, hence permitting their contributions to A_t to be considered by simple additivity as defined in Eq. (1). However, interaction of some RNA-binding proteins with fluorescent RNA substrates may alter quantum yield, possibly through direct contact with the fluorophore, by altering fluorophore solvent accessibility, or possibly through changes in local RNA structure, ionic strength, or pH. In our experience, the simplest

solutions in these instances are to either change the fluorophore (eg: Fl to Cy3 or TAMRA), move the fluorescent dye to a different location on the RNA substrate (eg: 3'-linkage in place of 5'), or add intervening nucleotides or carbon spacers to increase the distance between the fluorophore and the protein-binding site. Failing this, quantitative solutions are still attainable for reversible, binary binding equilibria by correction of the fractional contributions of free and bound RNA to A_t based on their relative quantum yields, given by Q_R and Q_{PR}, respectively[26, 32]:

$$\frac{[PR]}{[R]} = \frac{A_t - A_R}{A_{PR} - A_t} \times \frac{Q_R}{Q_{PR}} = \frac{A_c - A_R}{A_{PR} - A_c} \qquad (11)$$

Rearrangement thus provides a solution for the quantum yield-corrected anisotropy (A_c) of each binding reaction:

$$A_c = \frac{A_R + [(A_t - A_R) / (A_{PR} - A_t)](Q_R / Q_{PR})(A_{PR})}{1 + [(A_t - A_R) / (A_{PR} - A_t)](Q_R / Q_{PR})} \qquad (12)$$

This parameter may then be employed in A_c *versus* [P] data sets to resolve equilibrium binding constants as described above.

10.2.2.3. Instrumentation for Measurement of Fluorescence Anisotropy

Measurement of fluorescence anisotropy requires a steady-state spectrofluorometer containing excitation and emission polarizers. Selection of excitation and emission wavelengths may be achieved using monochromators or optical filters. For each binding reaction, fluorescence emission must be measured using polarizers fixed in both parallel (I_{VV}: vertical excitation polarizer, vertical emission polarizer) and perpendicular (I_{VH}: vertical excitation polarizer, horizontal emission polarizer) orientations. In the conventional "L" spectrofluorometer format, this requires two separate measurements, while "T" format instruments, which contain two independent photodetectors, permit both parameters to be measured simultaneously. Anisotropy is then calculated as:

$$A_t = \frac{I_{VV} - G \cdot I_{VH}}{I_{VV} + 2G \cdot I_{VH}} \qquad (13)$$

G is a correction factor that compensates for differences in the detection efficiency of vertically- *versus* horizontally-polarized light, and is calculated using steady-state fluorescence as $G = I_{HV}/I_{HH}$[25].

In our hands, routine measurement of fluorescence anisotropy has been greatly simplified using the Beacon 2000 Variable Temperature Fluorescence Polarization System, manufactured by Panvera (Madison, WI). Utility of this instrument is far more limited in scope than conventional spectrofluorometers, although several features make the Beacon an attractive and relatively inexpensive tool for anisotropy measurements. First, the Beacon is supplied with fluorescein excitation (λ_{max} = 485 nm) and emission (λ_{max} = 535 nm)

filters, which are optimized to permit very sensitive detection of fluorescein-conjugated biomolecules. Using Fl-tagged RNA substrates, we can reliably measure fluorescence anisotropy at concentrations approaching 10^{-10} M. However, additional filters must be purchased separately for detection of fluorescence at other wavelengths. Using the 6 mm × 50 mm sample holder with disposable glass tubes, we measure RNA-protein binding reactions in a total volume of 100 µl, at temperatures ranging from 6º to 65ºC. The Beacon measures fluorescence in all required polarizer orientations in a single operation, and returns measurements of total fluorescence intensity and anisotropy, with blank subtraction performed automatically if selected. The high sensitivity and small sample size permitted by this instrument greatly facilitate generation of the large data sets necessary for resolution of complex RNA-protein binding mechanisms.

10.2.3. Assessment of RNA Folding by FRET

The conformational heterogeneity and flexibility of RNA molecules significantly contribute to the often complex nature of their function. For example, the catalytic activities of ribozymes are intimately dependent on adoption of correct three-dimensional RNA structures[33-35], and protein-binding events may depend on presentation of RNA substrates in specific conformations[36-40]. Complex structures including pseudoknots contribute to the regulation of ribosomal frameshifting[41-43]. Furthermore, changes in system temperature, pH, cation population, and protein binding events can all potentially modulate the stability and/or dynamics of RNA folding[30, 39, 44-48].

Fluorescence resonance energy transfer (FRET) is emerging as a powerful tool in the elucidation of RNA folding mechanisms[49-51], due in part to the increasing ease with which fluorophores may be site-specifically conjugated within complex RNA molecules. We routinely evaluate folding of small (< 40 bases) RNA substrates by selectively labeling their 3'-termini with Fl and 5'-termini with Cy3 (Figure 10.4). The utility of this

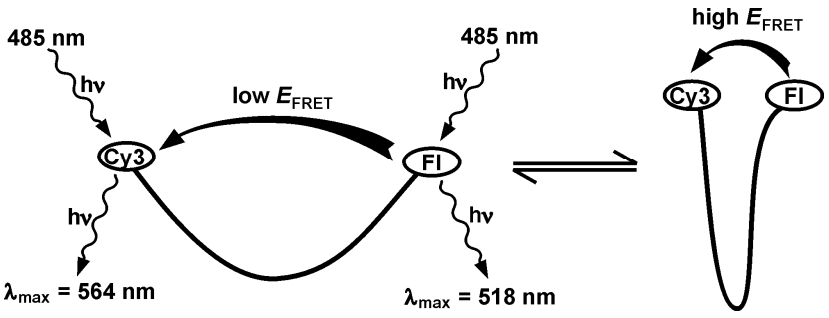

Figure 10.4. Measurement of RNA folding by FRET between conjugated 3'-Fl and 5'-Cy3 moieties. Changes in the distance between the termini in the unfolded (left) *versus* folded (right) states are detected by differences in FRET efficiency.

method is underscored by the relationship between the efficiency of FRET (E_{FRET}) and the scalar distance (r) between a fluorescent donor and acceptor:

$$E_{FRET} = R_0^6/(R_0^6 + r^6), \quad (14)$$

R_0 is the Förster distance for the donor-acceptor pair, defined as the distance at which FRET efficiency is 50%[25, 49]. In the case of the Fl-Cy3 fluorophore pair conjugated to single-stranded DNA, R_0 has been calculated as 55.7 Å[52]. We have also employed Fl-Cy5 as a donor-acceptor pair (R_0 = 47 Å) for measurements involving shorter RNA substrates[53], although many other options exist given the plethora of fluorophores available for RNA conjugation (Section 2).

We typically calculate E_{FRET} for double-labeled RNA substrates by measuring the decrease in fluorescence emission of the FRET donor in the presence of the acceptor[25, 50, 54].

$$E_{FRET} = 1 - (F_{DA}/F_D) \quad (15)$$

F_{DA} is the blank-corrected fluorescence of the donor in the presence of the acceptor, measured using a double-labeled RNA substrate (λ_{ex} = 490 nm and λ_{em} = 518 nm for fluorescein donors), while F_D is the fluorescence of the donor in the absence of the acceptor, measured using an RNA labeled only with Fl. Since quantum emission from donor moieties is not decreased by FRET in RNA substrates lacking acceptors, it is important that the labeling efficiency of the acceptor be very high (> 90%) for optimal resolution of E_{FRET}. This factor is particularly significant if estimates of inter-fluorophore distance are to be generated using Eq. (14). It has been our experience that custom oligoribonucleotides synthesized by commercial suppliers are more efficiently labeled at their 5'-termini, rather than using 3'-linkages. As such, we typically direct suppliers to conjugate FRET acceptor dyes to the 5'-end of synthetic RNA substrates. Alternatively, we have achieved efficient 3'-linkage through periodate oxidation and hydrazide coupling[29], although this must be performed in the absence of other tethered fluorophores to prevent oxidative damage to the dye, thus requiring ligation across single-stranded DNA splints (Figure 10.2) to generate the double-labeled RNA substrate.

In our lab, FRET has proven useful for measuring the thermal stability of folded RNA structures, cation-dependence of RNA folding, and local conformational changes induced by protein binding events. Selected examples of these experiments and some of the molecular details that they have revealed are outlined in Section 3.

10.3. ELUCIDATION OF MECHANISMS CONTRIBUTING TO REGULATION OF CYTOPLASMIC mRNA TURNOVER BY FLUORESCENCE SPECTROSCOPY

In eukaryotes, gene expression is a highly regulated process exhibiting control at many levels to ensure that gene products are maintained within levels appropriate for cellular growth and function. A critical determinant governing the synthetic rates of proteins are the concentrations of cytoplasmic mRNAs encoding them. As with any biological system, the steady-state level of a cytoplasmic mRNA is dependent on its rates of

both synthesis and degradation. The production rate of a cytoplasmic mRNA is a cumulative function of transcription, pre-mRNA processing, and nucleo-cytoplasmic transport, each of which may be subject to independent regulatory control. Cytoplasmic mRNA turnover is also tightly regulated, with mammalian mRNAs displaying a spectrum of decay rates spanning up to two orders of magnitude. Generally, determinants of both constitutive and inducible mRNA turnover rates are present as *cis*-acting sequences within individual mRNAs[55, 56].

AU-rich elements (AREs) constitute a varied family of RNA sequences localized to the 3'-untranslated regions (3'UTRs) of many labile mRNAs[24, 57]. The ability of AREs to modulate mRNA decay rates is mediated by association of cytoplasmic *trans*-acting factors [14]. Some proteins, like AUF1[58-60], tristetraprolin[61, 62], and KSRP[63], promote rapid decay of ARE-containing transcripts, while some others, including members of the Hu family of RNA-binding proteins, prevent mRNA degradation[64, 65]. Given the heterogeneity in size and sequence of AREs from different mammalian mRNAs, together with the plethora of cytoplasmic factors competing for these *cis*-acting elements, two of our principal research foci have been to characterize the substrate preferences of selected ARE-binding factors, and evaluate the structural and functional consequences of these *cis*-*trans* interactions. The following subsections describe some findings contributing to our understanding of this regulatory system, and the involvement of fluorescence spectroscopic techniques in these studies.

10.3.1. Evaluation of *Trans*-factor Binding Mechanisms and Affinity by Fluorescence Anisotropy

AUF1 was first identified as an activity capable of accelerating the decay of ARE-containing mRNAs in a cell-free system[66]. Subsequent purification and cloning revealed that AUF1 is expressed as a family of four protein isoforms through alternative splicing of a common pre-mRNA[67, 68]. The isoforms are denoted by their apparent molecular weights as $p37^{AUF1}$, $p40^{AUF1}$, $p42^{AUF1}$, and $p45^{AUF1}$, and all possess some degree of ARE-binding activity[68]. The $p42^{AUF1}$ and $p45^{AUF1}$ isoforms are exclusively nuclear in most cell types, while $p37^{AUF1}$ and $p40^{AUF1}$ are typically found in both nuclear and cytoplasmic compartments[67,69]. In numerous biochemical and cell biological systems, the expression and ARE-binding activity of $p37^{AUF1}$ and $p40^{AUF1}$ are closely associated with the rapid turnover of ARE-containing mRNAs[58-60, 70-72].

Our current model suggests that AUF1 binding to an ARE substrate functions as a targeting system to recruit subsequent components of the cytoplasmic mRNA decay machinery to the mRNA[73]. However, the RNA sequence and/or structural determinants that promote AUF1 binding to one ARE over another remain unclear. To gain insight into this question, we characterized the association of recombinant AUF1 proteins with a number of model RNA substrates. By GMSA, $p37^{AUF1}$ binding to the core ARE from tumor necrosis factor α (TNFα) mRNA forms two protein:RNA complexes in a concentration-dependent manner[19]. Hydrodynamic studies and chemical cross-linking indicated that $p37^{AUF1}$ is a dimer in solution, but forms protein tetramers on the TNFα ARE substrate, and larger oligomeric structures in the presence of longer ARE sequences[19, 74]. Using fluorescence anisotropy-based assays, we demonstrated that $p37^{AUF1}$ binding to the TNFα ARE substrate was consistent with the sequential association of protein dimers

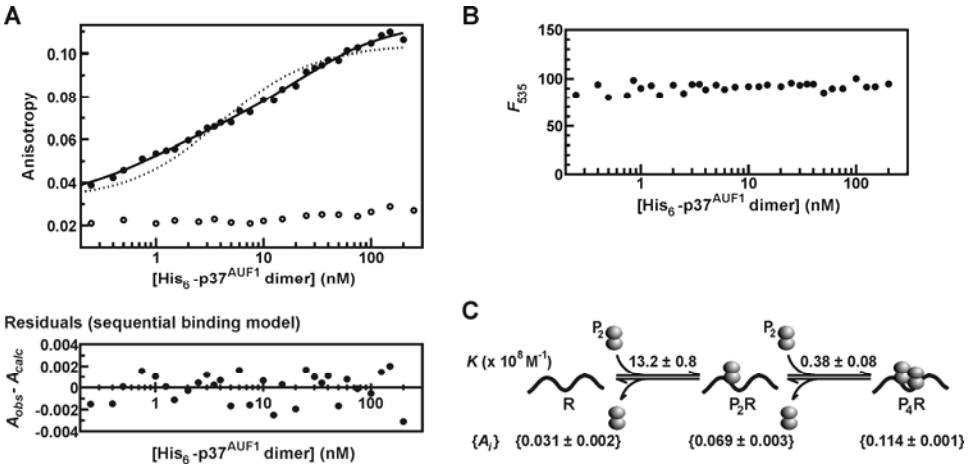

Figure 10.5. Assessment of p37^{AUF1} binding to RNA substrates by fluorescence anisotropy. (A) Anisotropy increases as a function of protein concentration for recombinant His$_6$-p37^{AUF1} binding to a fluorescent substrate containing the TNFα ARE sequence (solid circles) but not to an unrelated β-globin RNA fragment (open circles). Binding to the ARE substrate is well resolved by a two-stage binding algorithm defined by Eq. (7) (solid line), while the single-site binding model of Eq. (6) is clearly inappropriate (dotted line). (B) Total fluorescence emission from the Fl-TNFα ARE substrate does not vary with protein concentration, indicating no significant change in probe quantum yield and validating use of algorithms derived from Eq. (1). (C) Association binding (K) and intrinsic anisotropy (A_i) constants for p37^{AUF1} association with the ARE substrate. Data are from Ref. 29.

(Figure 10.5). Furthermore, this method allowed us to determine the equilibrium association constants describing both stages of AUF1 tetramer assembly on this substrate. Binding is not explicitly specific for the ARE sequence, since p37^{AUF1} also binds to polyuridylate RNA sequences with high affinity[19, 29]. Additional studies verified that p40^{AUF1} binds the TNFα ARE by a comparable mechanism, but that the affinity of p40^{AUF1} for this substrate is regulated by phosphorylation at two distinct sites[75]. Finally, the ability of AUF1 proteins to bind RNA is regulated by the structural presentation of each target site (described in Section 3.2), thus adding a new dimension to the complexity of RNA substrate selectivity by this *trans*-acting factor.

The inducible 70 kDa heat shock protein, Hsp70, has also been implicated as an ARE-binding factor and was identified in a common cytoplasmic complex with AUF1 by co-immunoprecipitation[76, 77]. Recombinant Hsp70 binding to the TNFα ARE was consistent with 1:1 stoichiometry by GMSA and fluorescence anisotropy-based assays, however, this protein formed cooperative, multimeric structures on polyuridylate substrates[78]. Solution of A_t *versus* [Hsp70] data sets for substrates containing a 32-nucleotide polyuridylate sequence resolved a Hill coefficient of 1.7 ± 0.1 (Figure 10.6). Unlike AUF1, however, association of Hsp70 with ARE substrates was not significantly influenced by conformational changes in the RNA. Together, these studies illustrated the mechanistic heterogeneity of ARE recognition by different ARE-binding proteins, and demonstrated that the selectivity of some proteins (ie: AUF1) but not others (ie: Hsp70) could be influenced by local higher order structures involving the RNA target site.

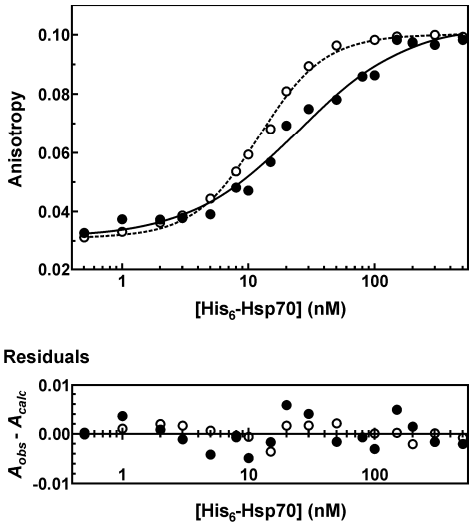

Figure 10.6. Association of recombinant Hsp70 with fluorescein-labeled RNA substrates containing the TNFα ARE resolved by Eq. (6) (solid circles, solid line) giving $K = 4.0 \pm 0.4 \times 10^7$ M^{-1} (K_d = 25 nM), or a 32-base polyuridylate sequence resolved by Eq. (9) (open circles, dashed line) giving $[Hsp70]_{1/2} = 12.2 \pm 0.4$ nM. Data are from Ref. 78.

10.3.2. Higher Order Structures Involving the TNFα ARE Regulate AUF1 Binding

The first indications that the TNFα ARE was capable of adopting a higher order RNA structure were based on an increase in the intrinsic anisotropy of fluorescein-labeled RNA substrates containing this element in the presence of Mg^{2+} [29], concomitant with inhibition of $p37^{AUF1}$ binding activity. Both inhibition of AUF1 binding and restriction of segmental RNA motion by Mg^{2+} were dependent on the ARE sequence, since neither effect was observed with the polyuridylate substrate. Subsequent experiments verified that the cation-induced structural change in the ARE substrate was an intramolecular event[29]. To more rigorously assess the mechanism and consequences of the Mg^{2+}-induced change in ARE structure, we synthesized selected RNA substrates with 3'-fluorescein and 5'-Cy3 moieties for conformational analyses by FRET[39]. Addition of Mg^{2+} to samples containing the double-labeled ARE substrate resulted in a large increase in E_{FRET} based on decreased emission from the fluorescein donor in the presence of the acceptor (Figure 10.7), indicating that the RNA termini are positioned closer together in solution in the presence of the cation. Similar to the measurements of segmental motion by fluorescence anisotropy, these cation-dependent changes in RNA folding were largely dependent on the ARE sequence, since the structure of a double-labeled polyuridylate substrate was only modestly affected by Mg^{2+}.

Thermal denaturation experiments indicated that the TNFα ARE is capable of forming a weak condensed structure in the absence of Mg^{2+}, but that this folding event is stabilized in the presence of the cation. The potential of different cations to stabilize the

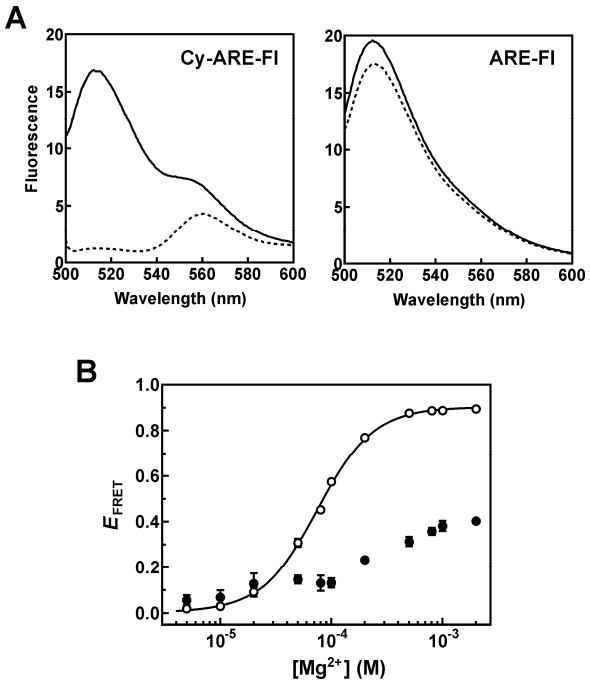

Figure 10.7. Assessment of RNA folding by FRET. (A) Emission spectra (λ_{ex} = 490 nm) of TNFα ARE RNA substrates labeled with FRET donor-acceptor pairs (Cy-ARE-Fl) or the donor alone (ARE-Fl) measured in the absence (solid line) or presence (dashed line) of 1 mM $MgCl_2$. (B) Mg^{2+} dependence of RNA folding measured for RNA substrates containing the TNFα ARE (open circles) or the 32-base polyuridylate sequence (solid circles). The cooperative nature of ARE folding with respect to Mg^{2+} was resolved using Eq. (9) (solid line), where $h = 1.7 \pm 0.1$ and $[Mg^{2+}]_{1/2} = 75 \pm 2$ μM. Data are from Ref. 39.

folded ARE structure was then assayed to help define a mechanistic basis for this effect. In all cases, adoption of the condensed RNA conformation was cooperative with respect to the cation ($h > 1$), but the ion concentrations necessary for stabilizing this structure varied widely. For example, an inorganic trivalent cation ($Co(NH_3)_6^{3+}$) stabilized the folded ARE at concentrations 1000-fold lower than inorganic, divalent cations (Mg^{2+}, Ca^{2+}, Mn^{2+}), and 1 million-fold lower than monovalent cations (Na^+, K^+). In addition, a cation where the positive charges are tightly packed ($Co(NH_3)_6^{3+}$) was 13-fold more effective at stabilizing the folded ARE than a comparably charged organic cation (spermidine^{3+}), where the positive charges are distributed across 11 Å. Based on the preference of the folded ARE for highly charged, condensed cations, we concluded that cations likely stabilize the folded ARE structure by targeted counterion neutralization at regions of high negative charge density[39]. To our knowledge, this represented the first indication that AREs may form higher-order RNA structures, and indicated that these structural transitions may have a significant impact on binding of *trans*-acting factors.

10.3.3. AUF1 Binding Modulates Local RNA Conformation

The FRET system was also used to determine whether association of AUF1 proteins with RNA substrates could modify local RNA structure. In the absence of Mg^{2+}, $p37^{AUF1}$ binding to the TNFα ARE resulted in a decrease in the scalar distance between the 5'- and 3'-termini, suggesting the adoption of a more condensed RNA structure. The folded structure appeared to be distinct from that stabilized by cations, however, since the FRET efficiency indicated a distance of 48-51 Å between the RNA termini, significantly larger than the 38 Å upper limit calculated for the cation-conjugated structure. Further evidence for this distinction was provided by measuring the protein-dependence of FRET in the presence of Mg^{2+}. At low protein concentrations, the RNA was tightly condensed, consistent with the cation-stabilized structure. However, as the protein concentration was increased, the distance between the RNA termini also increased, again resolving to the 48-51 Å range characteristic of the AUF1:ARE complex in the absence of Mg^{2+}. This

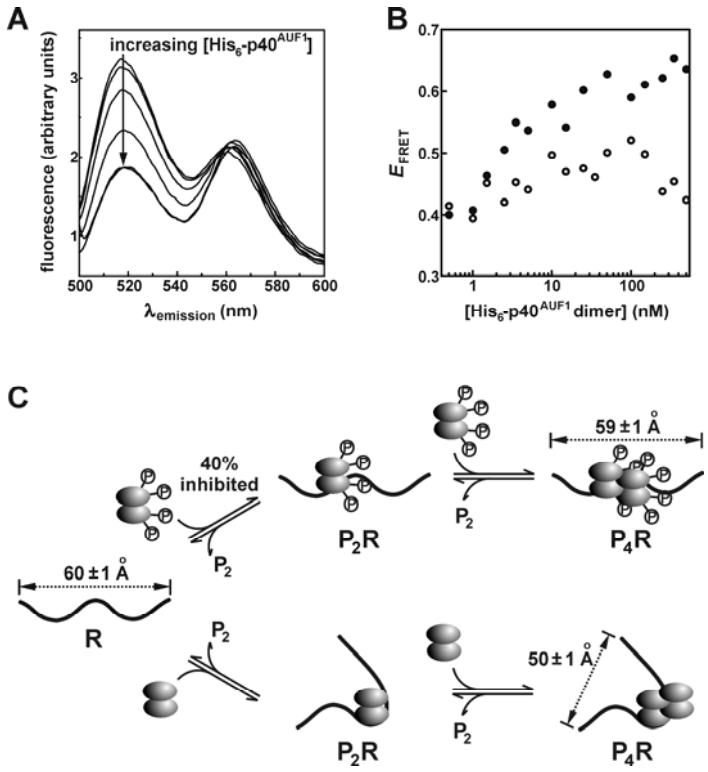

Figure 10.8. (A) Emission spectra (λ_{ex} = 490 nm) of the 5'-Cy3/3'-Fl labeled TNFα ARE RNA substrate under conditions of increasing recombinant $p40^{AUF1}$ concentration. (B) FRET efficiency as a function of $p40^{AUF1}$ concentration for the unphosphorylated protein (solid circles) compared with $p40^{AUF1}$ phosphorylated on Ser83 and Ser87 (open circles). (C) Schematic showing the assembly of $p40^{AUF1}$ tetramers on the TNFα ARE RNA substrate, and the roles of phosphorylation on the affinity and structural consequences of this process. Data are from Ref. 75.

result indicated that, at high protein concentrations, the structural influence of AUF1 binding can override cation-stabilized condensation of ARE conformation, and supported our previous hypothesis that oligomerization of AUF1 on the TNFα ARE converges to a common complex regardless of the presence of Mg^{2+} [29]. Finally, AUF1 association with a polyuridylate substrate also induced a change in RNA structure, similar to that observed with the ARE substrate. Together, these data indicated that while ion-stabilized ARE structural changes appear to be RNA sequence-dependent, AUF1-induced RNA folding is an RNA sequence-independent consequence of protein binding[39].

A physiological role for AUF1-induced RNA folding was suggested by parallel studies involving $p40^{AUF1}$. In the monocytic leukemia cell line THP-1, activation of the protein kinase C pathway with phorbol esters induced rapid but transient expression of ARE-containing mRNAs encoding the cytokine interleukin-1β and the inflammatory mediator TNFα, in part through a 6- to 12-fold increase in the stability of each transcript[79]. Concomitant with inhibition of mRNA turnover, changes were observed in the distribution of cytoplasmic ARE-binding complexes containing AUF1. Purification of AUF1 from polysome complexes revealed that stabilization of the ARE-containing transcripts was accompanied by loss of phosphate from Ser83 and Ser87 of $p40^{AUF1}$. Fluorescence anisotropy and FRET-based experiments using recombinant $p40^{AUF1}$ phosphorylated at these sites revealed that local remodeling of ARE structure is inhibited by $p40^{AUF1}$ phosphorylation (Figure 10.8). Interestingly, phosphorylation of both sites is required to inhibit AUF1-induced changes in RNA conformation; selective modification at Ser83 or Ser87 individually did not prevent adoption of a folded state[75]. Taken together, these data suggest that ARE-directed mRNA decay may be regulated in part through reversible phosphorylation of $p40^{AUF1}$ by modification of local RNA structure flanking the AUF1 binding site, possibly by selectively promoting or inhibiting subsequent factor recruitment.

10.4. FUTURE DIRECTIONS

In our hands, fluorescence anisotropy and FRET-based techniques have made vital contributions to our ongoing studies of ARE-directed mRNA turnover, and have permitted the perusal of mechanistic questions that would not have been otherwise feasible. On a broader scale, owing largely to the ease with which fluorescent-labeled RNA substrates may now be procured, many other labs are now applying similar techniques to a wide range of questions directed at understanding the intricate relationships between RNA structure and function.

Given the demonstrated utility of fluorescence-based assay systems in the study of RNA metabolism, coupled with the wealth of instrumentation and analysis tools available to investigators today, emerging studies will greatly benefit from the current state of the art in fluorescence technology. For example, time resolved fluorescence permits highly detailed analyses of RNA folding events by allowing explicit detection of localized conformational states. This strategy was applied to the cap region of the iron response element to reveal base-specific transitions between stacked and unstacked conformations[80]. In addition, time resolved FRET is a powerful method for assessing the distribution of distances between two points across a population of molecules. This methodology has recently been employed to detect RNA residues critical for ribozyme folding[81] and dy-

namic features of an essential subdomain of the hepatitis C virus internal ribosome entry site[82]. Finally, the emerging development and application of single molecule fluorescence spectroscopy is permitting conformational events involving individual RNA molecules to be visualized in real time. For example, folding and catalytic events have been visualized for individual ribozyme molecules[83, 84], providing heretofore unobservable perspectives of structural and dynamic processes within these RNAs, and opening a new frontier for quantitative assessment of macromolecular functions without statistical thermodynamics.

10.5. ACKNOWLEDGEMENTS

Funding for our projects is provided by NCI Grant R01 CA102428 from the National Institutes of Health and a Scientist Development Grant from the American Heart Association. Additional funding for the Center for Fluorescence Spectroscopy is provided by NCRR Grant P41 RR08119 from the National Institutes of Health.

10.6. REFERENCES

1. A. G. Vitreschak, D. A. Rodionov, A. A. Mironov, and M. S. Gelfand, Riboswitches: the oldest mechanism for regulation of gene expression? *Trends Genet.* **20**, 44-50 (2004).
2. G. Storz, J. A. Opdyke, and A. Zhang, Controlling mRNA stability and translation with small, noncoding RNAs. *Curr. Opin. Microbiol.* **7**, 140-144 (2004).
3. T. A. Steitz and P. B. Moore, RNA, the first macromolecular catalyst: The ribosome is a ribozyme. *Trends Biochem. Sci.* **28**, 411-418 (2003).
4. D. M. J. Lilley, The origins of RNA catalysis in ribozymes. *Trends Biochem. Sci.* **28**, 495-501 (2003).
5. M. Rajendran and A. D. Ellington, In vitro selection of molecular beacons. *Nucleic Acids Res.* **31**, 5700-5713 (2003).
6. T. Hermann and D. J. Patel, Adaptive recognition by nucleic acid aptamers. *Science* **287**, 820-825 (2000).
7. J. A. Doudna, A molecular contortionist. *Nature* **388**, 830 (1997).
8. A. E. Johnson, H. J. Adkins, E. A. Matthews, and C. R. Cantor, Distance moved by transfer RNA during translocation from the A site to the P site on the ribosome. *J. Mol. Biol.* **156**, 113-140 (1982).
9. J. Czworkowski, O. W. Odom, and B. Hardesty, Fluorescence study of the topology of messenger RNA bound to the 30S ribosomal subunit of *Escherichia coli*. *Biochemistry* **30**, 4821-4830 (1991).
10. P. Z. Qin and A. M. Pyle, Site-specific labeling of RNA with fluorophores and other structural probes. *Methods* **18**, 60-70 (1999).
11. Y.-T. Yu, Construction of 4-thiouridine site-specifically substituted RNAs for cross-linking studies. *Methods* **18**, 13-21 (1999).
12. C. G. Burd and G. Dreyfuss, Conserved structures and diversity of functions of RNA-binding proteins. *Science* **265**, 615-621 (1994).
13. J. E. G. McCarthy and H. Kollmus, Cytoplasmic mRNA-protein interactions in eukaryotic gene expression. *Trends Biochem. Sci.* **20**, (1995).
14. G. M. Wilson and G. Brewer, The search for trans-acting factors controlling messenger RNA decay. *Prog. Nucleic Acids Res. Mol. Biol.* **62**, 257-291 (1999).
15. L. E. Maquat, Nonsense-mediated mRNA decay: splicing, translation and mRNP dynamics. *Nature Rev. Mol. Cell Biol.* **5**, 89-99 (2004).
16. G. M. Wilson and G. Brewer, Identification and characterization of proteins binding A+U-rich elements. *Methods* **17**, 74-83 (1999).
17. W.-J. Ma, S. Cheng, C. Campbell, A. Wright, and H. Furneaux, Cloning and characterization of HuR, a ubiquitously expressed elav-like protein. *J. Biol. Chem.* **271**, 8144-8151 (1996).

18. C. T. DeMaria and G. Brewer, AUF1 binding affinity to A+U-rich elements correlates with rapid mRNA degradation. *J. Biol. Chem.* **271**, 12179-12184 (1996).
19. G. M. Wilson, Y. Sun, H. Lu, and G. Brewer, Assembly of AUF1 oligomers on U-rich RNA targets by sequential dimer association. *J. Biol. Chem.* **274**, 33374-33381 (1999).
20. I. Wong and T. M. Lohman, A double-filter method for nitrocellulose-filter binding: application to protein-nucleic acid interactions. *Proc. Natl. Acad. Sci. USA* **90**, 5428-5432 (1993).
21. P. S. Katsamba, S. Park, and I. A. Laird-Offringa, Kinetic studies of RNA-protein interactions using surface plasmon resonance. *Methods* **26**, 95-104 (2002).
22. A. Sadana, A kinetic study of analyte-receptor binding and dissociation, and dissociation alone, for biosensor applications: a fractal analysis. *Anal. Biochem.* **291**, 34-47 (2001).
23. W. J. Checovich, R. E. Bolger, and T. Burke, Fluorescence polarization - a new tool for cell and molecular biology. *Nature* **373**, 254-256 (1995).
24. G. Brewer, Characterization of c-*myc* 3' to 5' mRNA decay activities in an *in vitro* system. *J. Biol. Chem.* **273**, 34770-34774 (1998).
25. J. R. Lakowicz, *Principles of Fluorescence Spectroscopy*, Kluwer Academic/Plenum, New York, NY (1999).
26. J. R. Lundblad, M. Laurance, and R. H. Goodman, Fluorescence polarization analysis of protein-DNA and protein-protein interactions. *Mol. Endocrinol.* **10**, 607-612 (1996).
27. D. M. Jameson and W. H. Sawyer, Fluorescence anisotropy applied to biomolecular interactions. *Methods Enzymol.* **246**, 283-300 (1995).
28. G. Weber, Polarization of the fluorescence of macromolecules 2. Fluorescent conjugates of ovalbumin and bovine serum albumin. *Biochem. J.* **51**, 155-167 (1952).
29. G. M. Wilson, K. Sutphen, K. Chuang, and G. Brewer, Folding of A+U-rich RNA elements modulates AUF1 binding: Potential roles in regulation of mRNA turnover. *J. Biol. Chem.* **276**, 8695-8704 (2001).
30. S. L. Heilman-Miller, D. Thirumalai, and S. A. Woodson, Role of counterion condensation in folding of the *Tetrahymena* ribozyme. I. Equilibrium stabilization by cations. *J. Mol. Biol.* **306**, 1157-1166 (2001).
31. P. S. Katsamba, D. G. Myszka, and I. A. Laird-Offringa, Two functionally distinct steps mediate high affinity binding of U1A protein to U1 hairpin II RNA. *J. Biol. Chem.* **276**, 21476-21481 (2001).
32. W. B. Dandliker, M.-L. Hsu, J. Levin, and B. R. Rao, Equilibrium and kinetic inhibition assays based upon fluorescence polarization. *Methods Enzymol.* **74**, 3-28 (1981).
33. R. Russell, I. S. Millett, M. W. Tate, L. W. Kwok, B. Nakatani, S. M. Gruner, S. G. Mochrie, V. Pande, S. Doniach, D. Herschlag, and L. Pollack, Rapid compaction during RNA folding. *Proc. Natl. Acad. Sci. USA* **99**, 4266-4271 (2002).
34. J. Pan, M. L. Deras, and S. A. Woodson, Fast folding of a ribozyme by stabilizing core interactions: evidence of multiple folding pathways in RNA. *J. Mol. Biol.* **296** , 133-144 (2000).
35. D. Gilley and E. H. Blackburn, The telomerase RNA pseudoknot is critical for the stable assembly of a catalytically active ribonucleoprotein. *Proc. Natl. Acad. Sci. USA* **96**, 6621-6625 (1999).
36. K. J. Addess, J. P. Basilion, R. D. Klausner, T. A. Rouault, and A. Pardi, Structure and dynamics of the iron responsive element RNA: Implications for binding of the RNA by iron regulatory binding proteins. *J. Mol. Biol.* **274**, 72-83 (1997).
37. Y. Ke, J. Wu, E. A. Leibold, W. E. Walden, and E. C. Theil, Loops and bulge/loops in iron-responsive element isoforms influence iron regulatory protein binding. *J. Biol. Chem.* **273**, 23637-23640 (1998).
38. L. B. Blyn, L. M. Risen, R. H. Griffey, and D. E. Draper, The RNA-binding domain of ribosomal protein L11 recognizes an rRNA tertiary structure stabilized by both thiostrepton and magnesium ion. *Nucleic Acids Res.* **28**, 1778-1784 (2000).
39. G. M. Wilson, K. Sutphen, M. Moutafis, S. Sinha, and G. Brewer, Structural remodeling of an A+U-rich RNA element by cation or AUF1 binding. *J. Biol. Chem.* **276**, 38400-38409 (2001).
40. P. Bouvet, F. H. T. Allain, L. D. Finger, T. Dieckmann, and J. Feigon, Recognition of pre-formed and flexible elements of an RNA stem-loop by nucleolin. *J. Mol. Biol.* **309**, 763-775 (2001).
41. C. A. Theimer and D. P. Giedroc, Equilibrium unfolding pathway of an H-type RNA pseudoknot which promotes programmed-1 ribosomal frameshifting. *J. Mol. Biol.* **289**, 1283-1299 (1999).
42. G. M. Wilson and G. Brewer, Slip-sliding the frame: programmed -1 frameshifting on eukaryotic transcripts. *Genome Res.* **9**, 393-394 (1999).

43. E. P. Plant, K. L. Muldoon Jacobs, J. W. Harger, A. Meskauskas, J. L. Jacobs, J. L. Baxter, A. N. Petrov, and J. D. Dinman, The 9-Å solution: How mRNA pseudoknots promote efficient programmed -1 frameshifting. *RNA* **9**, 168-174 (2003).
44. P. E. Cole, S. K. Yang, and D. M. Crothers, Conformational changes of transfer ribonucleic acid. Equilibrium phase diagrams. *Biochemistry* **11**, 4358-4368 (1972).
45. J. Flinders and T. Dieckmann, A pH controlled conformational switch in the cleavage site of the VS ribozyme substrate RNA. *J. Mol. Biol.* **308**, 665-679 (2001).
46. T. C. Gluick, R. B. Gerstner, and D. E. Draper, Effects of Mg^{2+}, K^{+}, and H^{+} on an equilibrium between alternative conformations of an RNA pseudoknot. *J. Mol. Biol.* **270**, 451-463 (1997).
47. L. G. Laing, T. C. Gluick, and D. E. Draper, Stabilization of RNA structure by Mg ions: Specific and non-specific effects. *J. Mol. Biol.* **237**, 577-587 (1994).
48. S. Bernacchi, S. Stoylov, E. Piemont, D. Ficheux, B. P. Roques, J. L. Darlix, and Y. Mely, HIV-1 nucleocapsid protein activates transient melting of least stable parts of the secondary structure of TAR and its complementary sequence. *J. Mol. Biol.* **317**, 385-399 (2002).
49. R. M. Clegg, Fluorescence resonance energy transfer and nucleic acids. *Methods Enzymol.* **211**, 353-388 (1992).
50. D. Klostermeier and D. P. Millar, RNA conformation and folding studied with fluorescence resonance energy transfer. *Methods* **23**, 240-254 (2001).
51. D. M. J. Lilley and T. J. Wilson, Fluorescence resonance energy transfer as a structural tool for nucleic acids. *Curr. Opin. Chem. Biol.* **4**, 507-517 (2000).
52. D. G. Norman, R. J. Grainger, D. Uhrín, and D. M. J. Lilley, Location of cyanine-3 on double-stranded DNA: Importance for fluorescence resonance energy transfer studies. *Biochemistry* **39**, 6317-6324 (2000).
53. B. Y. Brewer, J. Malicka, P. J. Blackshear, and G. M. Wilson, RNA sequence elements required for high affinity binding by the zinc finger domain of tristetraprolin: Conformational changes coupled to the bipartite nature of AU-rich mRNA-destabilizing motifs. *J. Biol. Chem.* **279**, 27870-27877 (2004).
54. P. Wu and L. Brand, Resonance energy transfer: Methods and applications. *Anal. Biochem.* **218**, 1-13 (1994).
55. J. Guhaniyogi and G. Brewer, Regulation of mRNA stability in mammalian cells. *Gene* **265**, 11-23 (2001).
56. C. J. Wilusz, M. Wormington, and S. W. Peltz, The cap to tail guide to mRNA turnover. *Nature Rev. Mol. Cell Biol.* **2**, 237-246 (2001).
57. C.-Y. A. Chen and A.-B. Shyu, AU-rich elements: characterization and importance in mRNA degradation. *Trends Biochem. Sci.* **20**, 465-470 (1995).
58. P. Loflin, C.-Y. A. Chen, and A.-B. Shyu, Unraveling a cytoplasmic role for hnRNP D in the *in vivo* mRNA destablization directed by the AU-rich element. *Genes Dev.* **13**, 1884-1897 (1999).
59. A. Lapucci, M. Donnini, L. Papucci, E. Witort, A. Tempestini, A. Bevilacqua, A. Niolin, G. Brewer, N. Schiavone, and S. Capaccioli, AUF1 is a *bcl-2* A+U-rich element-binding protein involved in *bcl-2* mRNA destabilization during apoptosis. *J. Biol. Chem.* **277**, 16139-16146 (2002).
60. B. Sarkar, Q. Xi, C. He, and R. J. Schneider, Selective degradation of AU-rich mRNAs promoted by the p37 AUF1 protein isoform. *Mol. Cell. Biol.* **23**, 6685-6693 (2003).
61. W. S. Lai, E. Carballo, J. M. Thorn, E. A. Kennington, and P. J. Blackshear, Interactions of CCCH zinc finger proteins with mRNA: Binding of tristetraprolin-related zinc-finger proteins to AU-rich elements and destabilization of mRNA. *J. Biol. Chem.* **275**, 17827-17837 (2000).
62. W. S. Lai, E. Carballo, J. R. Strum, E. A. Kennington, R. S. Phillips, and P. J. Blackshear, Evidence that tristetraprolin binds to AU-rich elements and promotes the deadenylation and destabilization of tumor necrosis factor alpha mRNA. *Mol. Cell. Biol.* **19**, 4311-4323 (1999).
63. C.-Y. Chen, R. Gherzi, S.-E. Ong, E. L. Chan, R. Raijmakers, G. J. M. Pruijn, G. Stoecklin, C. Moroni, M. Mann, and M. Karin, AU binding proteins recruit the exosome to degrade ARE-containing mRNAs. *Cell* **107**, 451-464 (2001).
64. S. S. Y. Peng, C.-Y. A. Chen, N. Xu, and A.-B. Shyu, RNA stabilization by the AU-rich element binding protein, HuR, an ELAV protein. *EMBO J.* **17**, 3461-3470 (1998).
65. X. C. Fan and J. A. Steitz, Overexpression of HuR, a nuclear-cytoplasmic shuttling protein, increases the *in vivo* stability of ARE-containing mRNAs. *EMBO J.* **17**, 3448-3460 (1998).
66. G. Brewer, An A+U-rich element RNA-binding factor regulates c-*myc* mRNA stability in vitro. *Mol. Cell. Biol.* **11**, 2460-2466 (1991).

67. W. Zhang, B. J. Wagner, K. Ehrenman, A. W. Schaefer, C. T. DeMaria, D. Crater, K. DeHaven, L. Long, and G. Brewer, Purification, characterization, and cDNA cloning of an AU-rich element RNA-binding protein, AUF1. *Mol. Cell. Biol.* **13**, 7652-7665 (1993).
68. B. J. Wagner, C. T. DeMaria, Y. Sun, G. M. Wilson, and G. Brewer, Structure and genomic organization of the human AUF1 gene : alternative pre-RNA splicing generates four protein isoforms. *Genomics* **48**, 195-202 (1998).
69. Y. Arao, R. Kuriyama, F. Kayama, and S. Kato, A nuclear matrix-associated factor, SAF-B, interacts with specific isoforms of AUF1/hnRNP D. *Arch. Biochem. Biophys.* **380**, 228-236 (2000).
70. J. S. Buzby, S. Lee, P. van Winkle, C. T. DeMaria, G. Brewer, and M. S. Cairo, Increased granulocyte-macrophage colony-stimulating factor mRNA instability in cord versus adult mononuclear cells is translation-dependent and associated with increased levels of A+U-rich element binding factor. *Blood* **88**, 2889-2897 (1996).
71. A. Pende, K. D. Tremmel, C. T. DeMaria, B. C. Blaxall, W. A. Minobe, J. A. Sherman, J. D. Bisognano, M. R. Bristow, G. Brewer, and J. D. Port, Regulation of the mRNA-binding protein AUF1 by activation of the β-adrenergic receptor signal transduction pathway. *J. Biol. Chem.* **271**, 8493-8501 (1996).
72. O. I. Sirenko, A. K. Lofquist, C. T. DeMaria, J. S. Morris, G. Brewer, and J. S. Haskill, Adhesion-dependent regulation of an A+U-rich element-binding activity associated with AUF1. *Mol. Cell. Biol.* **17**, 3898-3906 (1997).
73. G. M. Wilson and G. Brewer, Regulation of mRNA stability by AUF1. In *RNA Binding Proteins: New Concepts in Gene Regulation* ed. by K. Sandberg and S. E. Molroney, pp 101-117. Kluwer Academic Publishers, Norwell, MA (2002).
74. C. T. DeMaria, Y. Sun, L. Long, B. J. Wagner, and G. Brewer, Structural determinants in AUF1 required for high affinity binding to A+U-rich elements. *J. Biol. Chem.* **272**, 27635-27643 (1997).
75. G. M. Wilson, J. Lu, K. Sutphen, Y. Suarez, S. Sinha, B. Brewer, E. C. Villanueva-Feliciano, R. M. Ylsa, S. Charles, and G. Brewer, Phosphorylation of $p40^{AUF1}$ regulates binding to A+U-rich mRNA-destabilizing elements and protein-induced changes in ribonucleoprotein structure. *J. Biol. Chem.* **278**, 33039-33048 (2003).
76. T. Henics, E. Nagy, H. J. Oh, C. Csermely, A. von Gabain, and J. R. Subjeck, Mammalian Hsp70 and Hsp110 proteins bind to RNA motifs involved in mRNA stability. *J. Biol. Chem.* **274**, 17318-17324 (1999).
77. G. Laroia, R. Cuesta, G. Brewer, and R. J. Schneider, Control of mRNA decay by heat shock-ubiquitin-proteosome pathway. *Science* **284**, 499-502 (1999).
78. G. M. Wilson, K. Sutphen, S. Bolikal, K. Chuang, and G. Brewer, Thermodynamics and kinetics of Hsp70 association with A+U-rich mRNA-destabilizing sequences. *J. Biol. Chem.* **276**, 44450-44456 (2001).
79. G. M. Wilson, J. Lu, K. Sutphen, Y. Sun, Y. Huynh, and G. Brewer, Regulation of A+U-rich element-directed mRNA turnover involving reversible phosphorylation of AUF1. *J. Biol. Chem.* **278**, 33029-33038 (2003).
80. K. B. Hall and D. J. Williams, Dynamics of the IRE RNA hairpin loop probed by 2-aminopurine fluorescence and stochastic dynamics simulations. *RNA* **10**, 34-47 (2004).
81. D. Klostermeier and D. P. Millar, Energetics of hydrogen bond networks in RNA: Hydrogen bonds surrounding G+1 and U42 are the major determinants for the tertiary structure stability of the hairpin ribozyme. *Biochemistry* **41**, 14095-14102 (2002).
82. S. E. Melcher, T. J. Wilson, and D. M. J. Lilley, The dynamic nature of the four-way junction of the hepatitis C virus IRES. *RNA* **9**, 809-820 (2003).
83. X. Zhuang, L. E. Bartley, H. P. Babcock, R. Russell, T. Ha, D. Herschlag, and R. Cuesta, A single-molecule study of RNA catalysis and folding. *Science* **288**, 2048-2051 (2000).
84. Z. Xie, N. Srividya, T. R. Sosnick, T. Pan, and N. F. Scherer, Single-molecule studies highlight conformational heterogeneity in the early folding steps of a large ribozyme. *Proc. Natl. Acad. Sci. USA* **101**, 534-539 (2004).